



## **Mineralogical research using hyperspectral Hyperion data in the vicinity of the Turkish Antarctic Research Station**

*Türk Antarktika Araştırma İstasyonu çevresinde hiperspektral Hyperion verileri kullanılarak mineralojik araştırma*

**MEHMET ALİ AKGÜL**<sup>1\*</sup> Orcid: 0000-0002-5517-9576

**SUPHİ URAL**<sup>2</sup> Orcid: 0000-0003-4865-011X

<sup>1</sup>*Geographic Information Systems Section, Department of Information Technologies, 6Th Regional Directorate, General Directorate of State Hydraulic Works, Adana, Turkey*

<sup>2</sup>*Department of Mining Engineering, Çukurova University, 01330, Adana, Turkey*

Geliş: 15.05.2023

Kabul: 31.05.2023

### **ABSTRACT**

Antarctica has a unique nature, unspoiled by the fact that it is almost completely covered by ice and there are no human community to influence it. The communities near Chile's southernmost tip, which is around 1200 km away, are the closest to the continent and include research stations belonging to various countries, including Türkiye. Because the stations are so remote from civilization, they must meet the needs of research stations on the mainland, which forces them to operate temporarily or with limited capability. The goal of this research was to explore the mineralogical structure around the Turkish Antarctic Research Station (TARS) in order to meet the station's demands, even if only partially. It is anticipated that these minerals can be exploited in this highly protected region, particularly in wastewater treatment systems for filtration or drinking water filtration, as well as for agricultural purposes to be carried out in unique conditions. Cloudiness, which is the largest weakness of optical satellites, as well as snow-covered regions that prohibit the ground from being seen, were considered in the archive scanning of this satellite, and the image dated 09.01.2020 was determined to be the best suited image. Jenny Island, the nearest land piece to the west, with a distance of 50 km to Horseshoe Island, where the TARS is located, was chosen as the research area among the land parts inside the Hyperion image. ENVI software was used for radiometric and atmospheric corrections of the Hyperion data used in the study. Mineral research was conducted using the Hyperspectral Material Identification (HMI) tool in the Tactical Hyperspectral Operations Resource (THOR) module of the same program. The USGS mineral database was used in the THOR HMI study

and the minerals with the best match were selected using the Adaptive Coherence Estimator (ACE) technique. As major minerals, corundum, diaspore, and montmorillonite minerals were detected in the coastal areas north of Jenny Island, albite-plagioclase and microcline-feldspar minerals gave anomalies in the rocky region of the island. Goethite ( $\alpha$ -FeO(OH)), hematite (Fe<sub>2</sub>O<sub>3</sub>), ferrihydrite ((Fe<sup>3+</sup>)<sub>2</sub>O<sub>3</sub>•0.5H<sub>2</sub>O), lepidocrosite ( $\gamma$ -FeO(OH)), limonite (FeO(OH)•nH<sub>2</sub>O), rutile (TiO<sub>2</sub>) and cuprite (Cu<sub>2</sub>O) minerals were detected in low concentrations.

**Keywords:** Hyperspectral Remote Sensing, Mineralogy, Jenny Island, Antarctic Peninsula

---

<sup>1\*</sup>Geographic Information Systems Section, Department of Information Technologies, 6th Regional Directorate, General Directorate of State Hydraulic Works, Adana, Turkey, mali.akgul@dsi.gov.tr

## ÖZ

Antarktika, neredeyse tamamen buzla kaplı olması ve onu etkileyecek hiçbir insan topluluğunun olmaması nedeniyle bozulmamış, eşsiz bir doğaya sahiptir. Türkiye'nin de aralarında bulunduğu çeşitli ülkelere ait araştırma istasyonları, Şili'nin en güney ucundaki yerleşimlerden yaklaşık 1200 km uzaklıkta yer almaktadır. İstasyonların yerleşim yerlerinden uzak olmasından dolayı ihtiyaçlarının anakaradan karşılanması gerekmekte olup bu durum istasyonları geçici veya sınırlı kapasiteyle çalışmaya zorlamaktadır. Bu araştırmanın amacı, Türkiye Antarktika Araştırma İstasyonunun (TARS) ihtiyaçlarını kısmen de olsa karşılayabilmek için istasyon çevresindeki mineralojik yapının incelenmesidir. Bu minerallerin yüksek derecede korunan bu bölgede, özellikle atık su arıtma sistemlerinin veya içme suyunun filtrasyonu için kullanılmasının yanı sıra, özel koşullarda gerçekleştirilecek tarımsal amaçlar için de değerlendirilebileceği öngörülmektedir. Uzaktan algılama ile yapılacak mineralojik çalışmalarda kullanılacak Hyperion uydusunun arşiv taramasında optik uyduların en büyük zayıflığı olan bulutluluk ve zeminin görülmesini engelleyen karla kaplı bölgeler dikkate alınmış ve 09.01.2020 tarihli görüntünün en uygun olduğu görülmüştür. Araştırma için uygun bulunan Hyperion görüntüsü içindeki kara parçalarından TARS'ın bulunduğu Horseshoe Adası'nın 50 km batısındaki en yakın kara parçası olan Jenny Adası seçilmiştir. Çalışmada kullanılan Hyperion verilerinin radyometrik ve atmosferik düzeltmeleri için ENVI yazılımı kullanılmıştır. Aynı programın THOR (Tactical Hyperspectral Operations Resource) modülünde yer alan HMI (Hyperspectral Material Identification) aracı kullanılarak mineral araştırması yapılmıştır. THOR HMI analizinde USGS mineral veri tabanı kullanılmış ve en iyi eşleşen mineraller ACE (Adaptive Coherence Estimator) tekniği kullanılarak seçilmiştir. Başlıca mineraller olarak, Jenny Adası'nın kuzeyindeki kıyı kesimlerinde Korindon, Diaspor ve Montmorillonit mineralleri belirlenirken, adanın kayalık bölgesinde Albit-plajiyoklaz ve Mikroclin-feldispat mineralleri anomaliler vermektedir. Götit ( $\alpha$ -FeO(OH)), Hematit (Fe<sub>2</sub>O<sub>3</sub>), Ferrihidrit ((Fe<sup>3+</sup>)<sub>2</sub>O<sub>3</sub>•0.5H<sub>2</sub>O), Lepidokrosit ( $\gamma$ -FeO(OH)), Limonit (FeO(OH)•nH<sub>2</sub>O), Rutil (TiO<sub>2</sub>) ve Kuprit (Cu<sub>2</sub>O) minerallerinin de düşük konsantrasyonlarda bulunduğu tespit edilmiştir.

**Anahtar Kelimeler:** *Hiperspektral Uzaktan Algılama, Mineraloji, Jenny Adası, Antarktika Yarımadası*

## **INTRODUCTION**

Discovered in 1820, Antarctica, differs from other continents because it is almost entirely covered with ice. Due to its untouched nature and the absence of a living society, our planet is a kind of memory. The closest settlements to the continent, which have research stations belonging to many countries, including Türkiye, are the settlements at the southernmost point of Chile, which is approximately 1200 km away. Being so far from civilization necessitates meeting the needs of research stations from the mainland, which causes the stations to operate temporarily or with minimal capability.

Edwards et al. (2004) reported detailed FT-Raman spectra studies of Beacon sandstone colonies in Antarctica, but characteristic orange-yellow surface color, cyanobacterial modification with hematite, goethite transformed from  $\alpha$ -Fe<sub>2</sub>O<sub>3</sub>,  $\alpha$ -FeOOH, attributed to the presence of iron (III) oxide hydroxide. Furthermore, due to their research, they concluded that the presence of iron oxide was compatible with distant spectroscopic-sensing investigations for Mars surface exploration.

Kelly et al. (2004) investigated the westernmost Oygarden Group islands of the Proterozoic Rayner Complex in Kemp Land, east of Antarctica. According to their findings, there were convincing evidence of the stable coexistence of high Mg-Al, silica-unsaturated metapelites, and orthopyroxene-corundum assemblages in natural rocks in this group of islands. They also discovered that orthopyroxene, corundum, sapphire, sillimanite, cordierite, garnet and kornepupine assemblages formed along a previously existent compositional zoning, resulting in different mineral Fe-Mg ratios.

In their study at the Artigas Antarctic Scientific Base on King George Island's Fildes Peninsula, Chacon et al. (2013) studied whether soil phosphorus cycle patterns alter between the glacial border and ice-free regions. They discovered that soil samples from the ice-free area had the highest amounts of iron/aluminum oxyhydroxides as well as the existence of secondary minerals such as hematite and the intergrade chlorite-vermiculite-montmorillonite.

Siqueira et al. (2023) attempted to create a new soil texture map for Antarctica by calculating the distribution of sand, silt, and clay in the ice-free major regions of Maritime Antarctica and the North Antarctic Peninsula. They examined multiple machine learning models using ancient soil texture data in their study and concluded that the random forest model produced the best results. They discovered that the maps they created had high spatial consistency, with soil texture dispersed according to parameters such as geomorphologies, parent material, and pedogenetic development.

The aim of this study was to examine the mineralogical structure around the Turkish Antarctic Research Station (TARS) so that the needs of the station may be met by themselves, even if partially. In this sensitively protected area, it was thought that these minerals could be used especially in wastewater treatment systems for filtration or drinking water filtration, as well as for agricultural purposes to be carried out in special environments.

## **MATERIAL AND METHOD**

### **Study Area**

As the study area, Jenny Island, which is the closest land piece to the west, with a distance of 50 km to Horseshoe Island, where the TARS is located, was chosen among the land parts within the Hyperion image (Figure 1).

The Island of Jenny, with the Island of Adelaide to the east, Leonie and Anchorage to the north, and Pourquoi Pas Island to the east, have altitudes of 298 and 569 m on the two highest peaks (Figure 2).

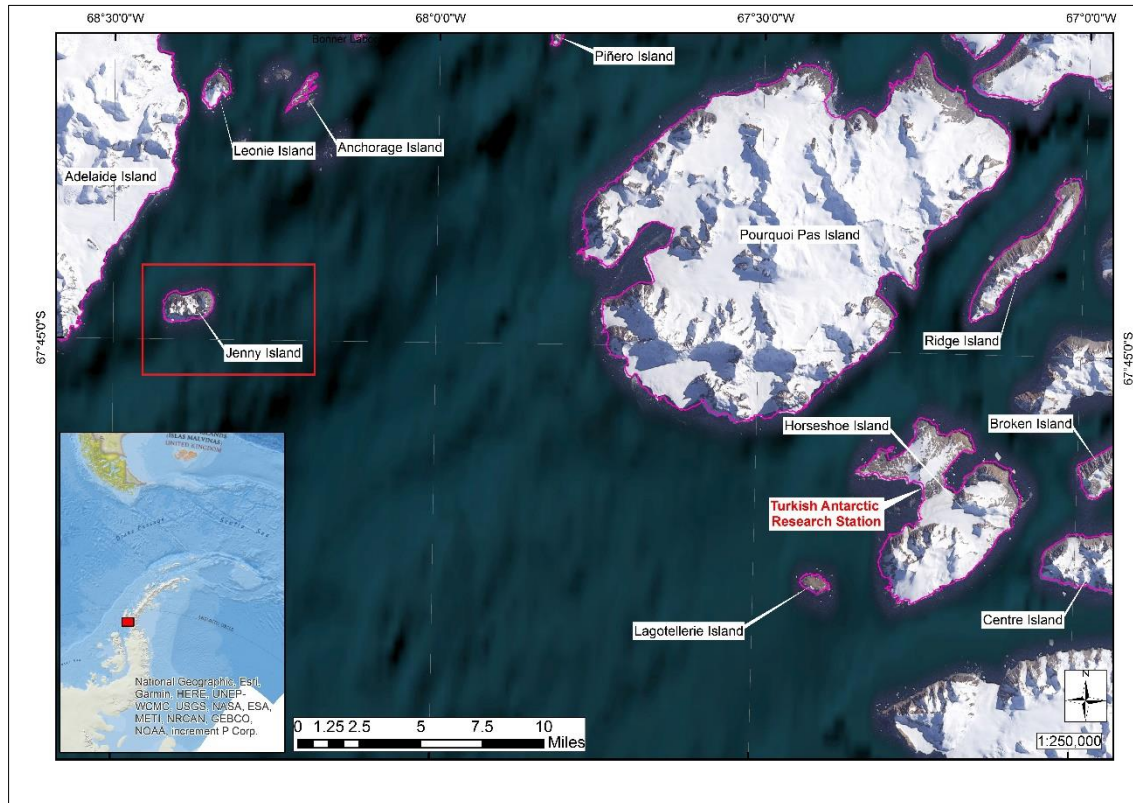


Figure 1. Study area.

Adelaide Island Intrusive Suite: Typically, granodiorite - gabbro hybrid plutons outcrop widely on the Wright Peninsula and the Mount Gaudry-Mount Mangin regions. Pluton compositions become increasingly silicic further north, with quartz monzonite and tonalite becoming more abundant. An emplacement age in the range, of 45 - 52 Ma, is favored (Pankhurst, 1982; Griffiths and Oglethorpe, 1998; Riley et al., 2012). Associated with the relatively minor dolerite intrusion. D-diorite; G-granite; Ga-gabbro; Gd-granodiorite; QD-quartz diorite; QM-quartz monzonite; To-tonalite (Figure 3). The mount Liotard Formation: up to 1800 m of basaltic andesite lavas, hyaloclastites, and breccias. Interbedded sedimentary rocks are rare or typically absent. The main areas of the outcrop are the Mount Liotard area, the Carvajal area, and Jenny Island. Probable correlation of the Bond Nunatak Formation. An age in the range of 75 - 65 Ma is likely and supported by Tertiary-age plant fossils from Cape Alexandra (Jefferson, 1980).

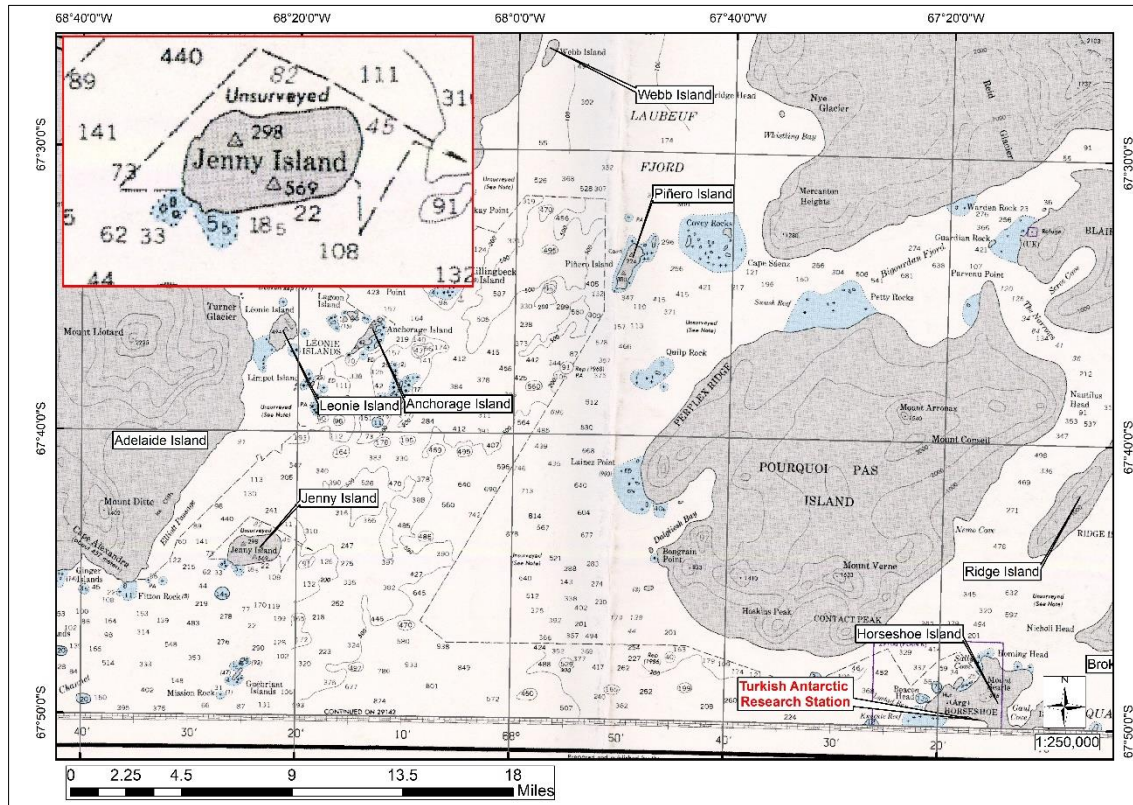


Figure 2. Hydrographic map (NGA, 1988).

According to Bastias et al. (2019), the deposition of Adelaide Island, which is located to the west of Jenny Island, documented the shift from deep sea sediment during the Late Jurassic period to shallower sediments and volcanic activity throughout the Cretaceous period (Figure 4).

### Material

The Earth Observing Mission-1 (EO-1) satellite, launched by the United States from Vandenberg Air Force Base on November 21, 2000, using a Delta II rocket, is the first spacecraft of the American New Millennium Program (NMP) (NASA, 2023). The EO-1 satellite has three instruments: the hyperspectral Hyperion instrument, which we employed in this work, the multispectral Advanced Land Imager (ALI) instrument, and the LEISA Atmospheric Corrector (LAC) instrument. The Hyperion instrument has a spatial resolution of 30 m and can detect 220 spectral bands ranging from 0.4 to 2.5  $\mu\text{m}$ . The ALI instrument is a multispectral sensor with the same spatial resolution as the Hyperion and can detect 10 spectral bands ranging from 0.4 to 2.4  $\mu\text{m}$ . The LAC instrument covers the 0.89-1.6  $\mu\text{m}$  wavelength IR band by means of a

wedged etalon filter and three arrays of In-Ga detectors, each array covering a spatial resolution of 250 m (Barry, 2001).

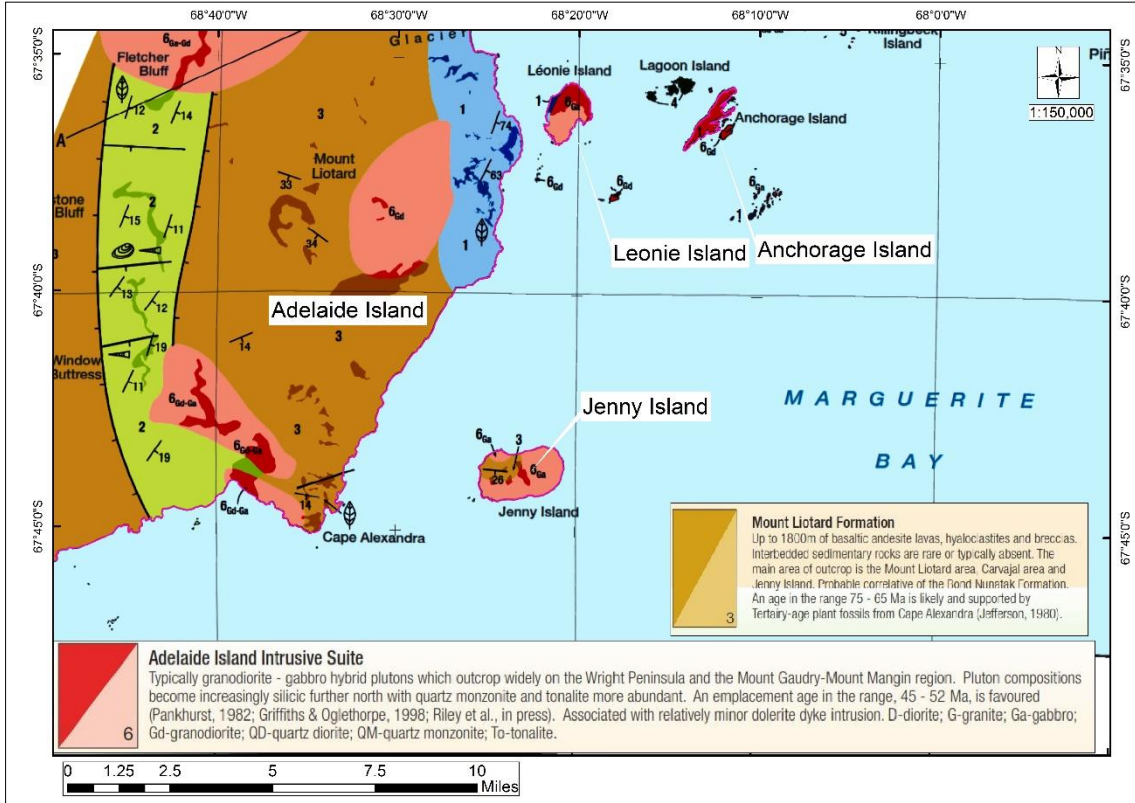


Figure 3. Study area geological map (Riley et al., 2011).

There are 220 unique spectral channels captured, with a total spectrum spans from 357 to 2576 nm. The Level 1 Radiometric product includes 242 bands in total, however only 198 of them are calibrated. There are only 196 unique channels due to the overlap between the VNIR and SWIR focal planes. Calibrated channels for the VNIR are 8-57 and 77-224 for the SWIR. The lack of calibration of all 242 channels is mostly due to the detectors' poor sensitivity. In certain channels, the uncalibrated bands are set to zero (Beck, 2003). The features of the Hyperion data used in the study are given in Table 1, and the footprint of the satellite is shown in Figure 5.

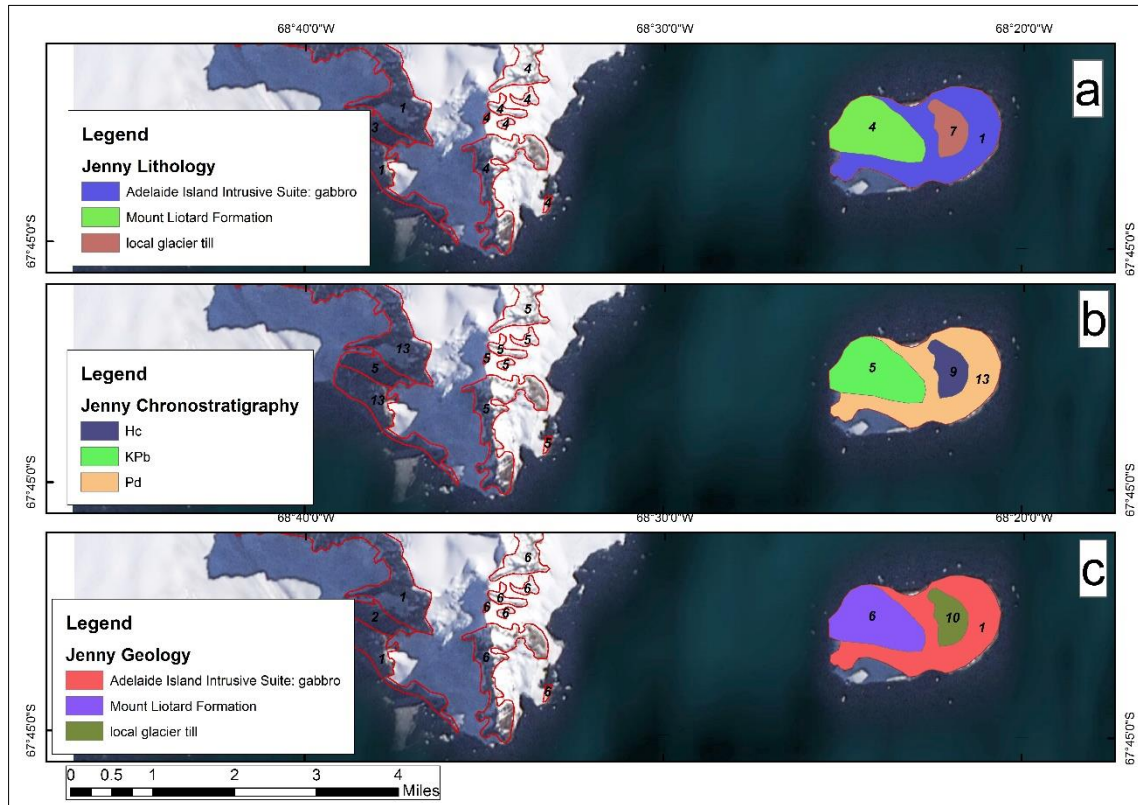


Figure 4. Jenny Island lithology, chronostratigraphy, and geology map (Bastias et al., 2019).

Table 1. Hyperion instrument specifications (Beck, 2003).

Instrument	Specifications	Instrument	Number Of Bands
Spectral Range	0.4-2.5 $\mu\text{m}$	Visible Bands	35
Spatial Resolution	30 m	Near Infrared Bands	35
Swath Width	7.5 km	Short Wave Infrared	172
Spectral Coverage	Continuous	Panchromatic Bands	0
Pan Band Resolution	N/A	Middle Infrared Bands	0
Stereo	no	Thermal Band	0
Number of Spacecraft	1	Total Bands	220
Temporal Resolution	200 days		

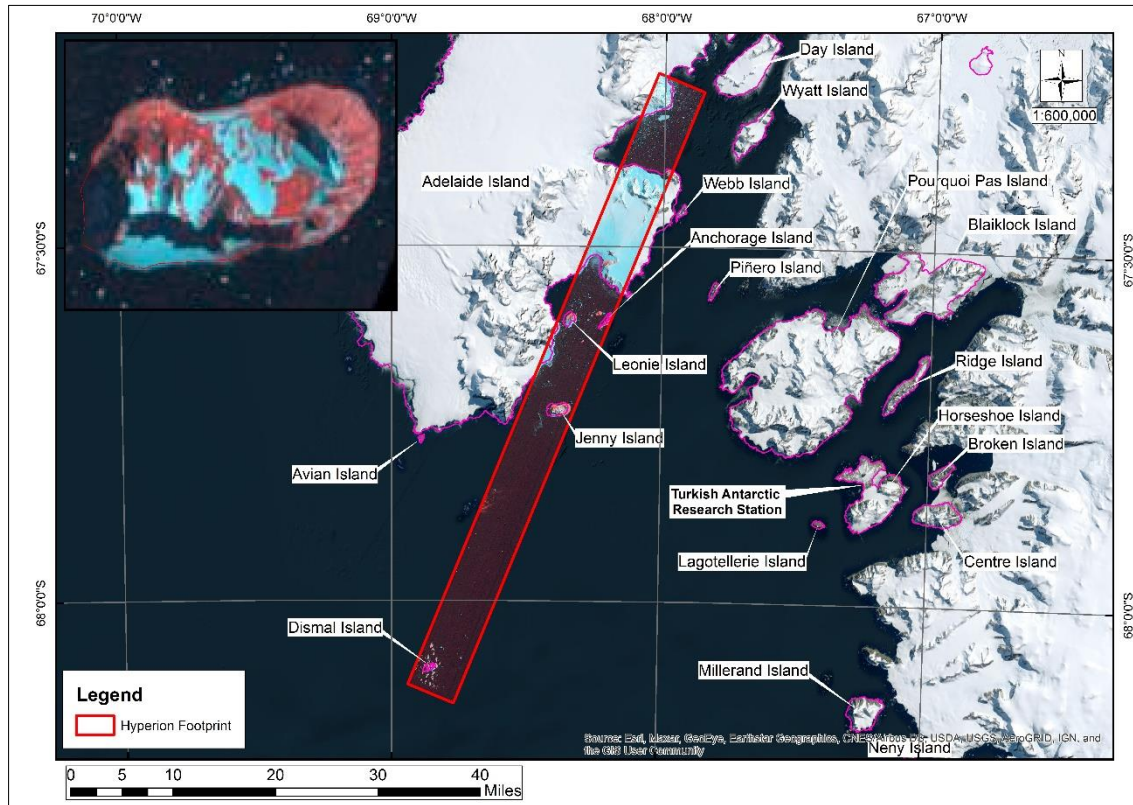


Figure 5. Hyperion image footprint.

Hyperion data are processed at three different levels: L1R, L1Gst, and L1T. While radiometric corrections of the images were made at the L1R level, in addition to the L1R level at the L1Gst level, a 90 m precision Digital Elevation Model (DEM) was used for topographic accuracy and systematic geometric corrections obtained from the spacecraft ephemeris data were applied. At the L1T level, in addition to the L1Gst level, radiometric and systematic geometric corrections including ground control points were applied for geodetic accuracy (Simon et al., 2006; USGS, 2021). In this study, since only the L1R and L1Gst levels of the study area are available, L1Gst data, which has increased topographic accuracy by using DEM data, was used in addition to the L1R level data. Hyperion data were obtained from <https://earthexplorer.usgs.gov/>, and the name and date of the image was given in Table 2.

Table 2. The name of Hyperion image and date, used in the study.

Image Name	Date
EO1H2201072010009110KF_SGS_01	01/09/2010

## Method

Environment for Visualizing Images (ENVI) software was used for radiometric and atmospheric corrections of Hyperion data, which can detect at 357 and 2576 nm wavelengths and 30 m resolution in 220 bands used in the study. ENVI is a software with advanced image processing methods that enables extracting meaningful information from many data it supports. In hyperspectral satellites, some bands can produce significant interference, particularly at wavelengths associated with atmospheric absorption and water vapor. These bands must be removed before analysis procedures. In EO-1 Hyperion data, bands 1-7, 58-76, and 221-242 are automatically set to 0 by the data provider (Barry, 2001). Also, as stated by Datt et al., (2003), the 121-126, and 167-180 bands were removed in the pretreatment step due to the strong noise generation corresponding to strong water vapor absorption.

After removing the bad bands, the radiometric corrections required for the use of the image were calculated with the ENVI software, and the Quick Atmospheric Correction (QUAC) module in the same software was used for the atmospheric corrections calculated according to Canty (2014). QUAC is a scene-based empirical method that converts radiance values to apparent surface reflectance. Scene-based means that the atmospheric correction parameters are derived strictly from the pixel spectra within the scene and not from any ancillary data (Bernstein et al., 2005; Bernstein et al., 2012). Mineral analysis from radiometrically and atmospherically corrected images was performed using the Hyperspectral Material Identification (HMI) tool in the Tactical Hyperspectral Operations Resource (THOR) module in the ENVI software. In the THOR HMI analysis, the mineral library belonging to the United States Geological Survey (USGS) was used and the minerals with the best match were determined according to the Adaptive Coherence Estimator (ACE) algorithm. The ACE algorithm is a method that measures whether the spectrum of any mineral in the library is a good match with the spectrum of a selected pixel in the image. The ACE algorithm is used for the mineral that is dense in the pixel.

ACE values range from -1 to 1, with values close to 1 indicating the best match. The research was conducted in accordance with the flow diagram shown in Figure 6.

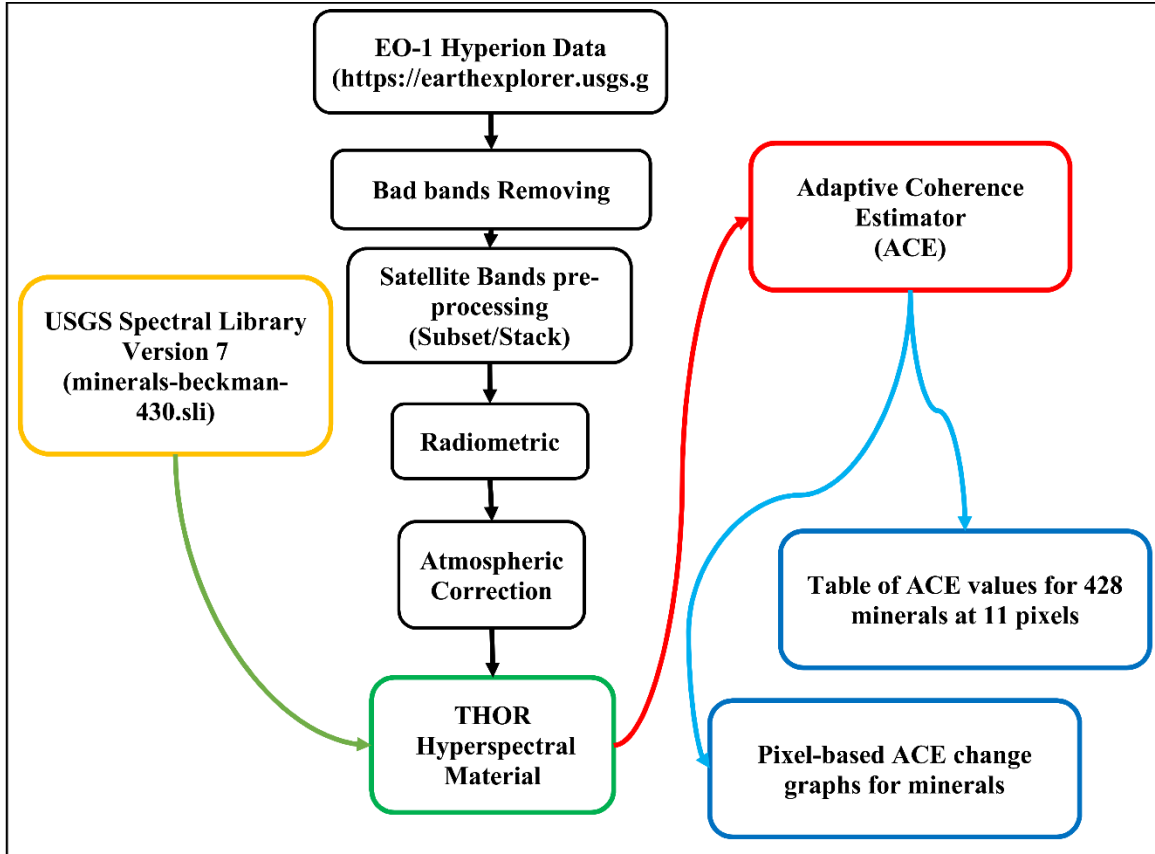


Figure 6. Flowchart of the study.

Pixel-based analysis was performed on the northern slopes of the island where there was no ice cover and rocky, and dirt ground were visibly combined. All of the Hyperion data pixels on this 470 m path from the top of the rock to the sea had been examined, and the total number of pixels is 11. While 7 of these pixels (about 300 m) were on rocky terrain, the remaining 4 pixels (about 170 m) were on sandy land. The map showing the location of the pixels were given in Figure 7.



Figure 7. Map showing the location of pixels.

## RESULTS

The pixels to be evaluated were numbered from the top of the rock on the island's north side to the sea. These numbers begin at the peak with 168\_62 and terminate at the seashore at 178\_52 (Figure 8). These values also specify the pixel coordinates of the image.

After numbering the pixels, the ACE values for each pixel were computed one by one for 428 minerals chosen from the USGS mineral database. The minerals with the highest ACE values in each pixel was listed in Table 3. ACE levels between 0.9 and 1.0 are very acceptable, good between 0.75 and 0.9, poor-appropriate between 0.5-0.75, and inappropriate for values less than 0.5 (L3HARRIS, 2023).

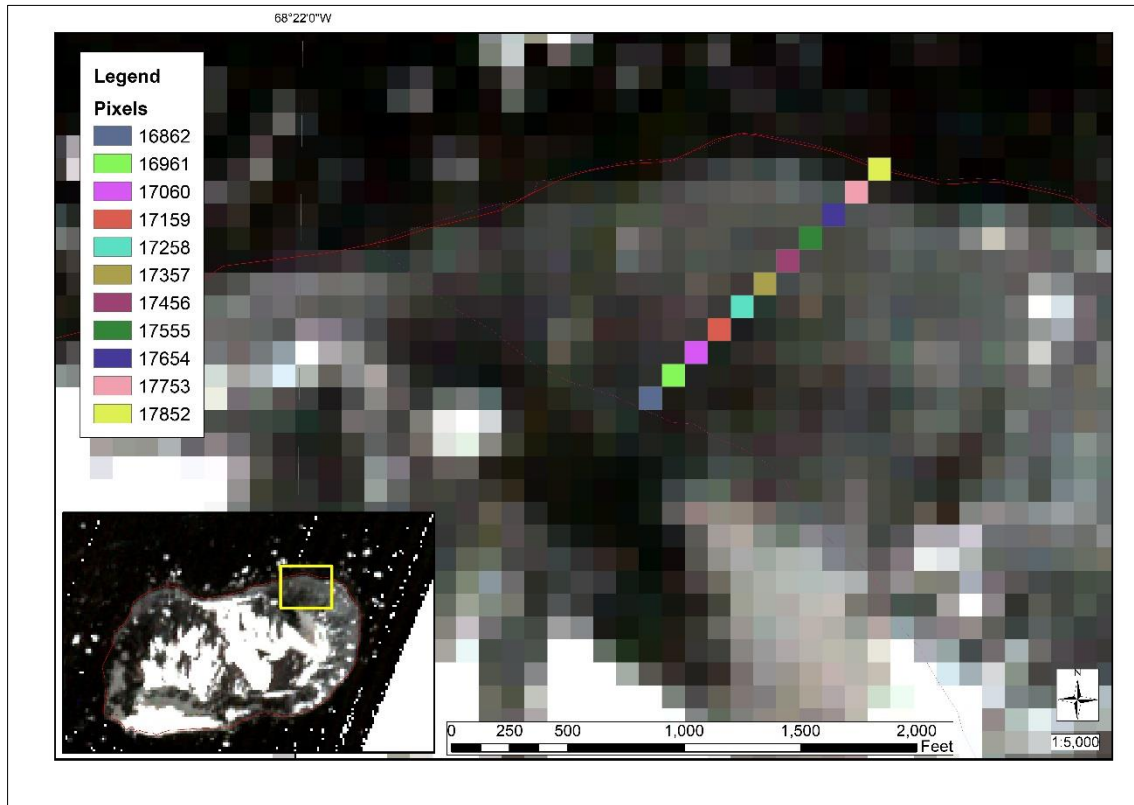


Figure 8. Map showing the location of analyzed Pixels.

Table 3. Results of ACE analysis.

Pixel ID	Signature Name	ACE value	Library Source
168_62	Limonite HS41.3	0.5462	minerals_beckman_430.sli
169_61	Strontianite HS272.3B	0.5265	minerals_beckman_430.sli
170_60	Illite IL101 (2M2)	0.5822	minerals_beckman_430.sli
171_59	Muscovite GDS120 Pegma M.	0.5565	minerals_beckman_430.sli
172_58	Sillimanite HS186.3B	0.5417	minerals_beckman_430.sli
173_57	Strontianite HS272.3B	0.6509	minerals_beckman_430.sli
174_56	Calcite WS272	0.6312	minerals_beckman_430.sli
175_55	Quartz HS117.3B Aventurin	0.5546	minerals_beckman_430.sli
176_54	Corundum HS283.3B	0.6709	minerals_beckman_430.sli

177_53	Quartz HS117.3B Aventurin	0.4144	minerals_beckman_430.sli
178_52	Nontronite NG-1.b <2um fr	0.3700	minerals_beckman_430.sli

The location of the analyzed pixels on the geological map was located in the Adelaide Island Intrusive Suite: gabbro unit (Figure 9).

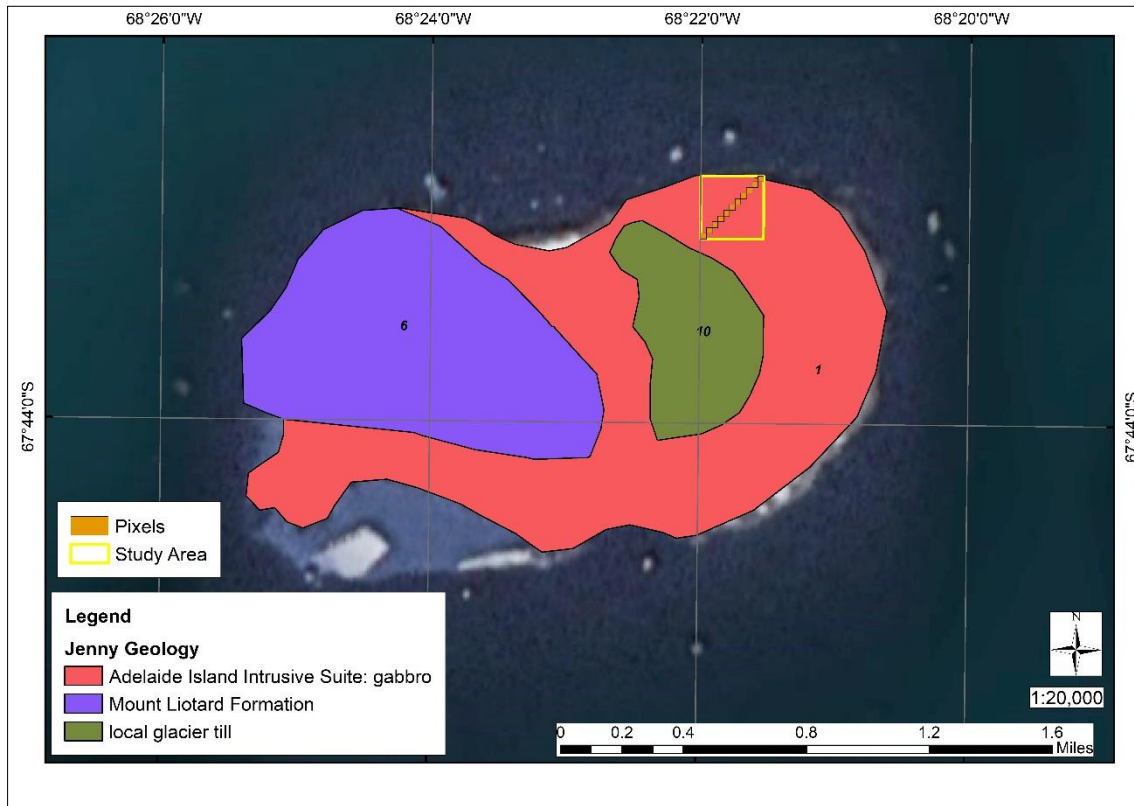


Figure 9. The location of the analyzed pixels on the geological map.

Figure 10 depicted the graph of the change obtained by calculating pixel-based ACE values for corundum and diaspore minerals. Although the ACE values in the two minerals were almost the same in the rocky land, the graph showed that it rised in the region of 85 m from the rocky region and then progressively falled toward the sea shore.

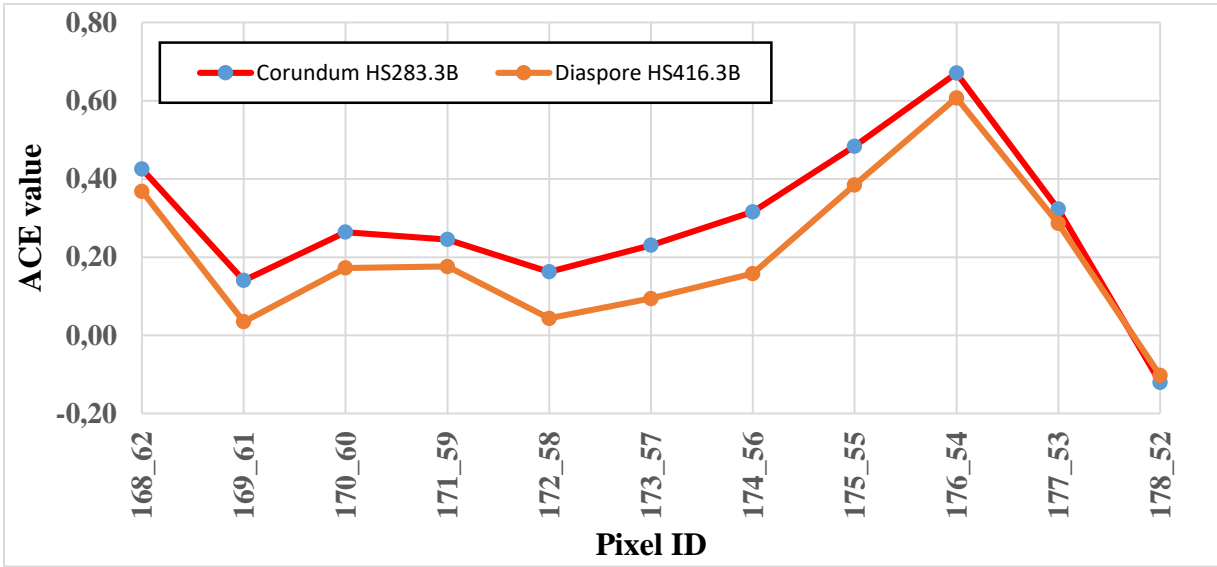


Figure 10. The graph of the pixel values of the corundum and diaspore minerals.

The pixel-based ACE change graph created for montmorillonite minerals was given in Figure 11. The ACE values of the montmorillonite minerals were the same as those of the corundum and diaspore minerals in the rocky zone, and then taken about the same values up to 85 m from the shore. The last two pixels approaching the coast were found to have a sharp reduction.

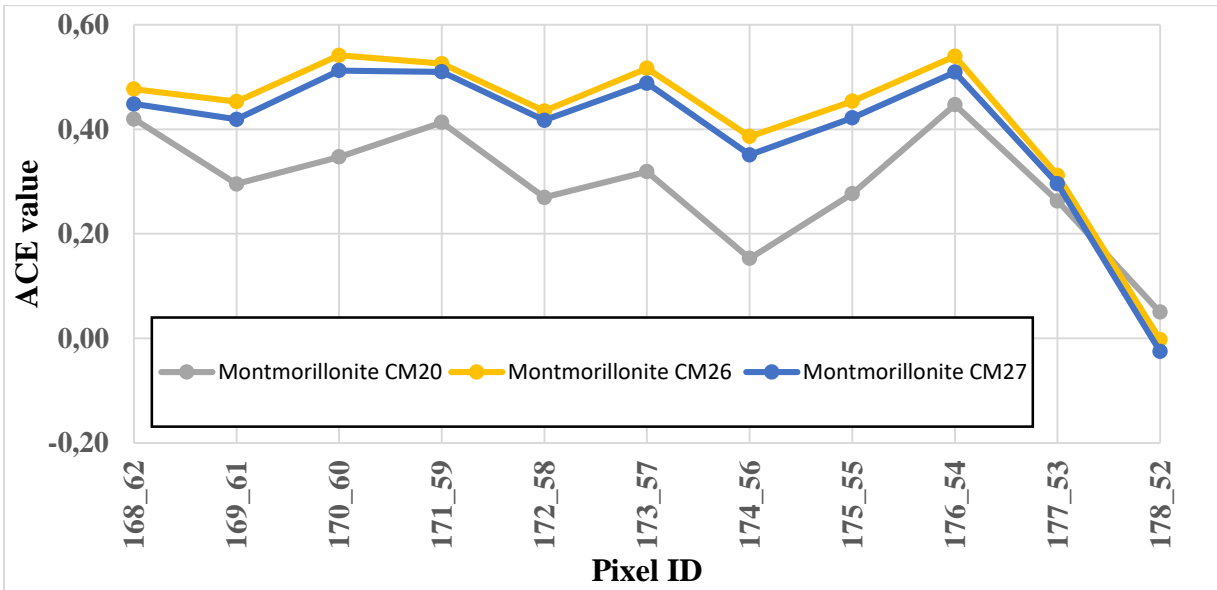


Figure 11. The graph of the pixel values of the montmorillonite mineral.

In addition, a pixel-based ACE change graph for the goethite minerals were created and shown in Figure 12. ACE values were found to be higher in the rocky terrain and lower towards the seashore. The coarse-grained goethite minerals were also more valuable in coastal locations than the medium-grained material.

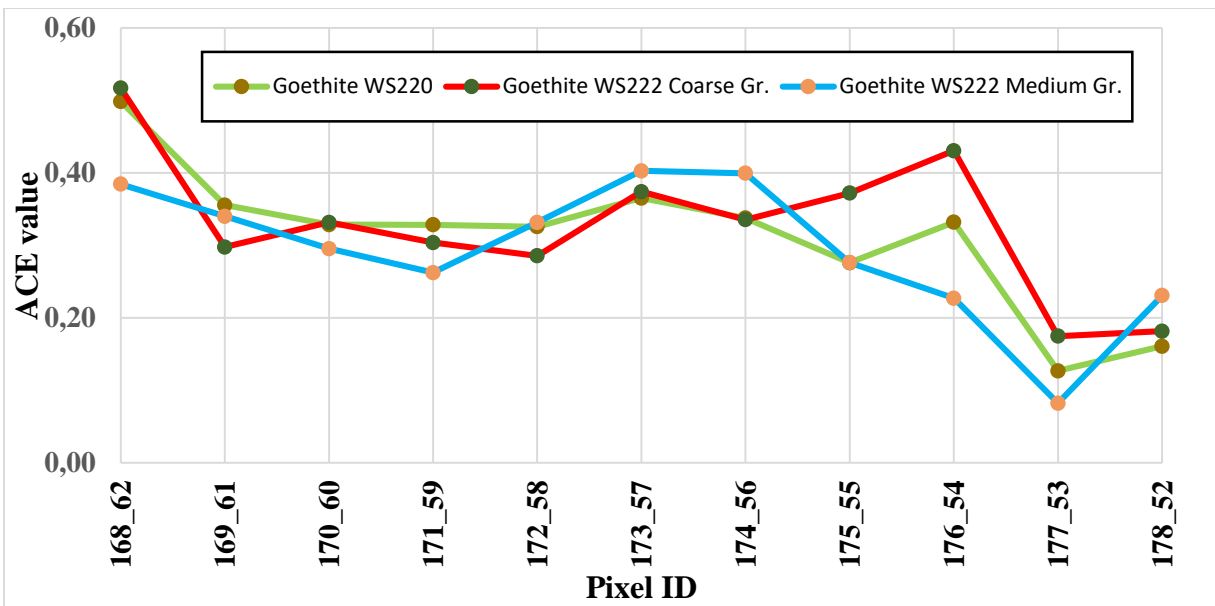


Figure 12. The graph of the pixel values of the goethite mineral.

Figure 13 depicted a pixel-based ACE change graph for the hematite minerals. ACE values were shown to be greater in rocky terrain and decreased toward the seaside, similar to the goethite minerals. Although the ACE value of the mineral appeared to grow in pixel number 178\_52, the final pixel on the shoreline, this was due to a portion of the pixel entering the sea.

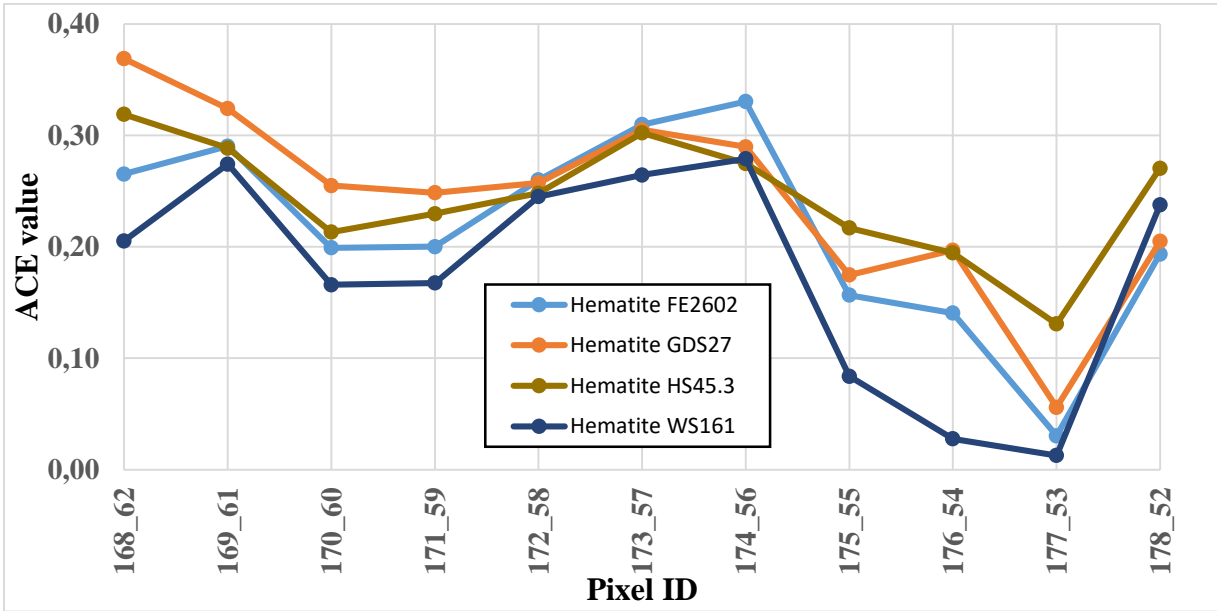


Figure 13. The graph of the pixel values of the hematite mineral.

The pixel-based ACE change graph for limonite given Figure 14. ACE values were greater in rocky terrain and dropped near the seashore, similar to goethite and hematite minerals.

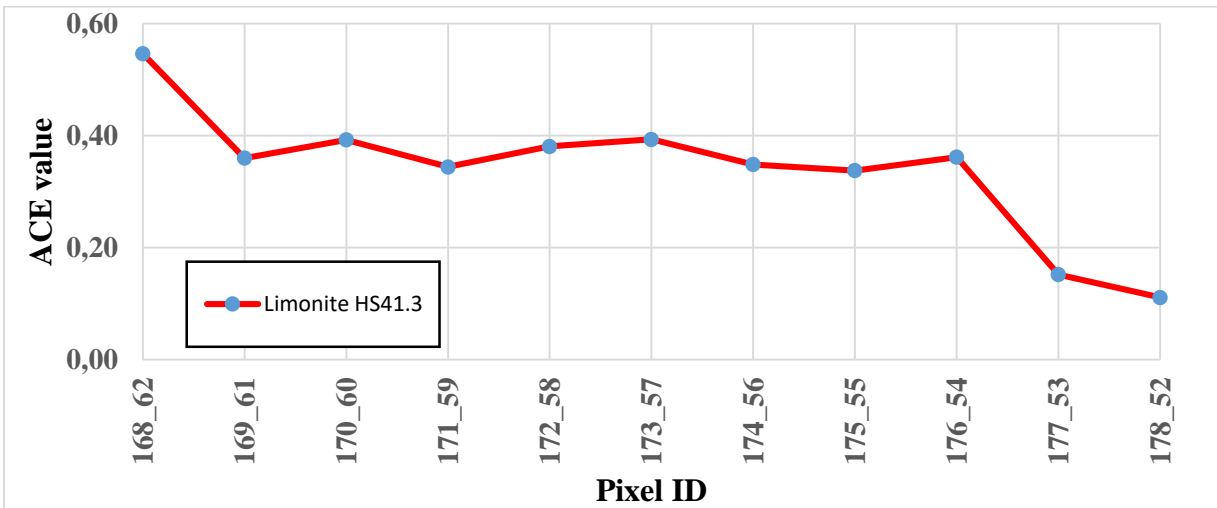


Figure 14. The graph of the pixel values of the limonite mineral.

As major minerals, while corundum, diaspore, and montmorillonite minerals were detected in the coastal areas north of Jenny Island, albite-plagioclase and microcline-feldspar minerals gave anomalies in the rocky region of the island. Goethite ( $\alpha$ -FeO(OH)), hematite ( $\text{Fe}_2\text{O}_3$ ), ferrihydrite ( $(\text{Fe}^{3+})_2\text{O}_3 \cdot 0.5\text{H}_2\text{O}$ ), lepidocrosite ( $\gamma$ -FeO(OH)), limonite ( $\text{FeO}(\text{OH}) \cdot n\text{H}_2\text{O}$ ), rutile ( $\text{TiO}_2$ ) and cuprite ( $\text{Cu}_2\text{O}$ ) minerals were detected in low concentrations.

## DISCUSSION

Antarctica is a form of memory of our planet owing to its untouched nature and the absence of human civilization to influence it. The nearest communities are in the southernmost tip of South America and house research stations from many countries, including Turkey. Because the stations are far from the nearest communities, the demands of the research stations must be addressed on a continuous basis, requiring them to function on a temporary or restricted basis. The research aimed to investigate the mineralogical structure surrounding the TARS and to partially satisfy the stations demands. Jenny Island, which is the nearest land piece to the west and approximately 50 km from Horseshoe Island, where the TARS is located, was chosen as the study area. The ACE technique was used in the study, which used the USGS mineral database, and as a result of the analyses, corundum, diaspore, and montmorillonite minerals were detected in the coastal parts of Jenny Island's northern part, while albite-plagioclase and microcline-feldspar minerals in the rocky part of the island gave anomalies. In addition, goethite ( $\alpha$ -FeO(OH)), hematite ( $\text{Fe}_2\text{O}_3$ ), ferrihydrite ( $(\text{Fe}^{3+})_2\text{O}_3 \cdot 0.5\text{H}_2\text{O}$ ), lepidocrosite ( $\gamma$ -FeO(OH)), limonite ( $\text{FeO}(\text{OH}) \cdot n\text{H}_2\text{O}$ ), rutile ( $\text{TiO}_2$ ) and cuprite ( $\text{Cu}_2\text{O}$ ) minerals were detected in low concentrations. It was thought that iron oxide minerals were formed as a result of weathering of monzonite with gabbro and granodiorite. Antarctica presents many challenges for geological research due to its remoteness, inaccessible location in many areas, and poorly exposed lithological units. Therefore, remote sensing applications are particularly useful when extreme environmental conditions limit the direct geological exploration. It is thought that EO-1 Hyperion satellite observations will help to better understand the mineralogy of regions not yet explored by terrestrial surveys in Antarctica, compared to remote sensing methods applied so far. According to the findings of the study, certain minerals discovered in this highly protected

location can be used for agricultural purposes in specific settings, as well as filtration or drinking water filtration, particularly in wastewater treatment systems.

**Conflicts of Interest:** The authors declare no conflicts of interest.

## REFERENCES

- Barry, P., 2001. EO-1/Hyperion Science Data User's Guide. TRW Space, Defense & Information Systems.
- Bastias, J., Calderón, M., Israel, L., Hervé, F., Spikings, R., Pankhurst, R., Castillo, P., Fanning, M., & Ugalde, R., 2019. The Byers Basin: Jurassic-Cretaceous tectonic and depositional evolution of the fore arc deposits of the South Shetland Islands and its implications for the northern Antarctic Peninsula. *International Geology Review*, 62(11), 1467-1484. <https://doi.org/10.1080/00206814.2019.1655669>.
- Beck, R., 2003. EO-1 User Guide v.2.3; University of Cincinnati: Cincinnati, Ohio, U.S., p.74.
- Bernstein, L.S., Adler-Golden, S.M., Sundberg, R.L., Levine, R.Y., Perkins, T.C., Berk, A., 2005. Validation of the QUick Atmospheric Correction (QUAC) algorithm for VNIR-SWIR multi- and hyperspectral imagery. *SPIE, Proceedings, Algorithms and Technologies for Multispectral, Hyperspectral, and Ultraspectral Imagery XI*. Vol. 5806, pp. 668-678.
- Bernstein, L.S., Jin, X., Gregor, B., Adler-Golden, S.M., 2012. Quick Atmospheric Correction Code: Algorithm Description and Recent Upgrades. *Optical Engineering* 51, No. 11 111719. <https://doi.org/10.1117/1.OE.51.11.111719>.
- Canty, J.M., 2014. *Image Analysis, Classification and Change Detection in Remote Sensing, with Algorithms for ENVI/IDL and Python.*, Third Edition. CRC Press.
- Chacon, N., Ascanio, M., Herrera, R., Benzo, D., Flores, S., Silva, S.J., García, B. 2013. Do P cycling patterns differ between ice-free areas and glacial boundaries in the Maritime Antarctic region? *Arctic, Antarctic, and Alpine Research*, 45, 190–200. <https://doi.org/10.1657/1938-4246-45.2.190>.

- Datt, B., McVicar, T.R., Van Niel, T.G., Jupp, D.L.B., 2003. Preprocessing EO-1 Hyperion Hyperspectral Data to Support the Application of Agricultural Indexes. *IEEE Transactions on Geoscience and Remote Sensing*, vol. 41, no. 6, pp. 1246-1259, June 2003, <https://doi.org/10.1109/TGRS.2003.813206>.
- Edwards, H.G.M., Wynn-Williams, D.D., Villar, S.E.J., 2004. Biological modification of haematite in Antarctic cryptoendolithic communities. *J. Raman Spectrosc.*, 35: 470-474. <https://doi.org/10.1002/jrs.1171>.
- Griffiths, C.J., Oglethorpe, R.D., 1998. The stratigraphy and geochronology of Adelaide Island. *Antarctic Science*, 10, 462-475.
- Jefferson, T.H., 1980. Angiosperm fossils in supposed Jurassic volcanogenic shales, Antarctica. *Nature*, 285, 187-188.
- Kelly, N.M., Harley, S.L., 2004. Orthopyroxene-corundum in Mg-Al-rich granulites from the Oygarden Islands, East Antarctica. *Journal of Petrology*, 45, 1481-1512. <https://doi.org/10.1093/petrology/egh023>.
- L3HARRIS, 2023. Hyperspectral Material Identification, <https://www.l3harrisgeospatial.com/docs/thorhyperspectralmaterialidentification.html>, Date of access: 05.05.2023.
- NASA, 2023. Catalog of Spaceborne Imaging, NASA Space Science Data Coordinated Archive (NSSDC), NASA Goddard Space Flight Center (GSFC), <https://nssdc.gsfc.nasa.gov/>, Date of access: 05.05.2023.
- NGA, 1988. Square Bay to Matha Strait Including Adelaide Island: Antarctica. United States, Defense Mapping Agency, Hydrographic/Topographic Center. National Geospatial-Intelligence Agency.
- Pankhurst, R.J., 1982. Rb-Sr geochronology of Graham Land, Antarctica. *Journal of the Geological Society, London*, 139, 701-711.
- Riley, T.R., Flowerdew, M.J., Haselwimmer, C.E., 2011. Geological Map of Adelaide Island, Graham Land (1:200 000 scale). BAS GEOMAP 2 Series, sheet 2, British Antarctic Survey, Cambridge, UK.
- Riley, T.R., Flowerdew, M.J., Whitehouse, M.J., 2012. Chrono- and lithostratigraphy of a Mesozoic–Tertiary fore- to intra-arc basin: Adelaide Island, Antarctic Peninsula. *Geological Magazine*, 149(5), 768-782. doi:10.1017/S0016756811001002.

Simon, K., and Beckman, T., 2006. Hyperion Level 1G (L1GST) Product Output Files Data Format Control Book (DFCB), Earth Observing-1 (EO-1), version 1.0, USGS Center for Earth Resource Observation and Science (EROS), Sioux Falls, South Dakota.

Siqueira, R.G., Moquedace, C.M., Francelino, M.R., Schaefer, C.E.G.R., Fernandes-Filho, E.I., 2023. Machine learning applied for Antarctic soil mapping: Spatial prediction of soil texture for Maritime Antarctica and Northern Antarctic Peninsula, *Geoderma*, vol:432, 116405, <https://doi.org/10.1016/j.geoderma.2023.116405>.

USGS, 2021. EO1 Data Dictionary. Earth Resources Observation and Science (EROS) Center July 2, 2021. <https://www.usgs.gov/centers/eros/science/eo1-data-dictionary>.